

# Diffusion coefficient of vacancies and jump length of electrons in $\text{Co}_{1-x}\text{Zn}_x\text{Fe}_2\text{O}_4$ ferrites

M. EL-SAADAWY\*

*Physics Department, Faculty of Science, Kafrelsheikh University, Kafrelsheikh City, Egypt*

Received May 31, 2011; Accepted April 22, 2012

© The Author(s) 2012. This article is published with open access at Springerlink.com

**Abstract:** A series of polycrystalline samples of  $\text{Co}_{1-x}\text{Zn}_x\text{Fe}_2\text{O}_4$  where ( $x = 0.1, 0.2, 0.3, 0.4, 0.5$  and  $0.6$ ) were prepared by the usual ceramic technique. X-ray diffraction patterns confirmed the spinel cubic structure. The diffusion coefficients of oxygen vacancies were estimated from dc conductivity measurements. It was noticed that the diffusion coefficient decreases with increasing  $\text{Zn}^{2+}$  concentrations. An increase of temperature increases the diffusion of lattice vacancies. The Curie temperature, lattice parameter and jump length of electrons were studied as a function of  $\text{Zn}^{2+}$  concentration. From the correlation between the ionic radius and the radii of octahedral and tetrahedral sites, the theoretical lattice parameters were calculated and suggested cation distribution for the given ferrites was determined.

**Key words:** diffusion coefficient; lattice parameter; jump length and jump rate of vacancies; Curie temperature; cation distribution

## 1 Introduction

Polycrystalline ferrites have high resistivity and low current losses play a useful role in many technological applications as transform cores [1] for microwave integrating circuits [2]. The physical properties of ferrites are dependent on the method of preparation and the amount and type of doping. A ferromagnetic spinel can be represented by the formula  $\text{AB}_2\text{O}_4$ , the A-B magnetic interactions between the magnetic atoms on the A (tetrahedral) site and the B (octahedral) sites are stronger than A-A interactions and B-B interactions [3]. Metallic atoms are in inverse distributions: half the atoms of iron are in the A sites and the other half, plus

magnetic atoms, in the B sites. However,  $\text{CoZnFe}_2\text{O}_4$  is not completely inverse, and the degree of inversion depends on the heat treatment. The spinel ferrite  $\text{MgFe}_{2-x}\text{Cr}_x\text{O}_4$  was also studied by Mossbauer spectroscopy over a wide range of temperatures [4]. The spinel ferrites  $\text{Zn}_x\text{Ni}_{5/3-x}\text{Fe}_1\text{Sb}_{1/3}\text{O}_4$  were also studied [5] by Mossbauer spectroscopy over a wide range of temperatures. Spectral studies for  $\text{Co}_x\text{Ni}_{5/3-x}\text{Sb}_{1/3}\text{Fe}_1\text{O}_4$  ferrite sintered at 1470 K for 4 h were performed [6]. The diffusion of oxygen atoms in Ni ferrite was studied using the nuclear microanalysis methods for determining the oxygen atoms concentration [7]. The diffusion coefficient of vacancies and jump length of electrons in  $\text{MgFe}_{2-x}\text{Cr}_x\text{O}_4$  ferrites were also studied [8]. This study has been performed to drive data on the oxygen tracer diffusion in ferrites. In addition, the diffusion information may be helpful in analyzing the structural

\* Corresponding author.

E-mail: elsaadawy2000@yahoo.com

defects in the oxygen sublattice. This study into diffusion may reinforce the existing concept that the diffusion of cation vacancies is faster than that of anions. These and other factors relating to the oxygen diffusion are important for understanding the process which takes place during the ferrite synthesis (thermal and thermomagnetic treatment and operations of ferrites).

## 2 Experimental

The high-purity powders of  $\text{Fe}_2\text{O}_3$ ,  $\text{CoO}$  and  $\text{ZnO}$ ,

were mixed in desired proportions, presintered at  $850^\circ\text{C}$  for 6 h and quenched to room temperature. Then the compositions were ground to very fine powder using an agate mortar. The powders were then pressed in the form of discs. After sintering at  $1150^\circ\text{C}$  for 12 h, the discs allowed to cool to room temperature and finally polished to achieve uniform parallel surfaces. Contact on the sample surface was made by silver paste. The completion of the solid state reaction was checked by X-ray diffraction using a Jeol JSX-60 PA XRD with  $\text{CoK}_\alpha$  radiation of wavelength  $\lambda = 1.7902 \text{ \AA}$ . The results revealed that all the samples

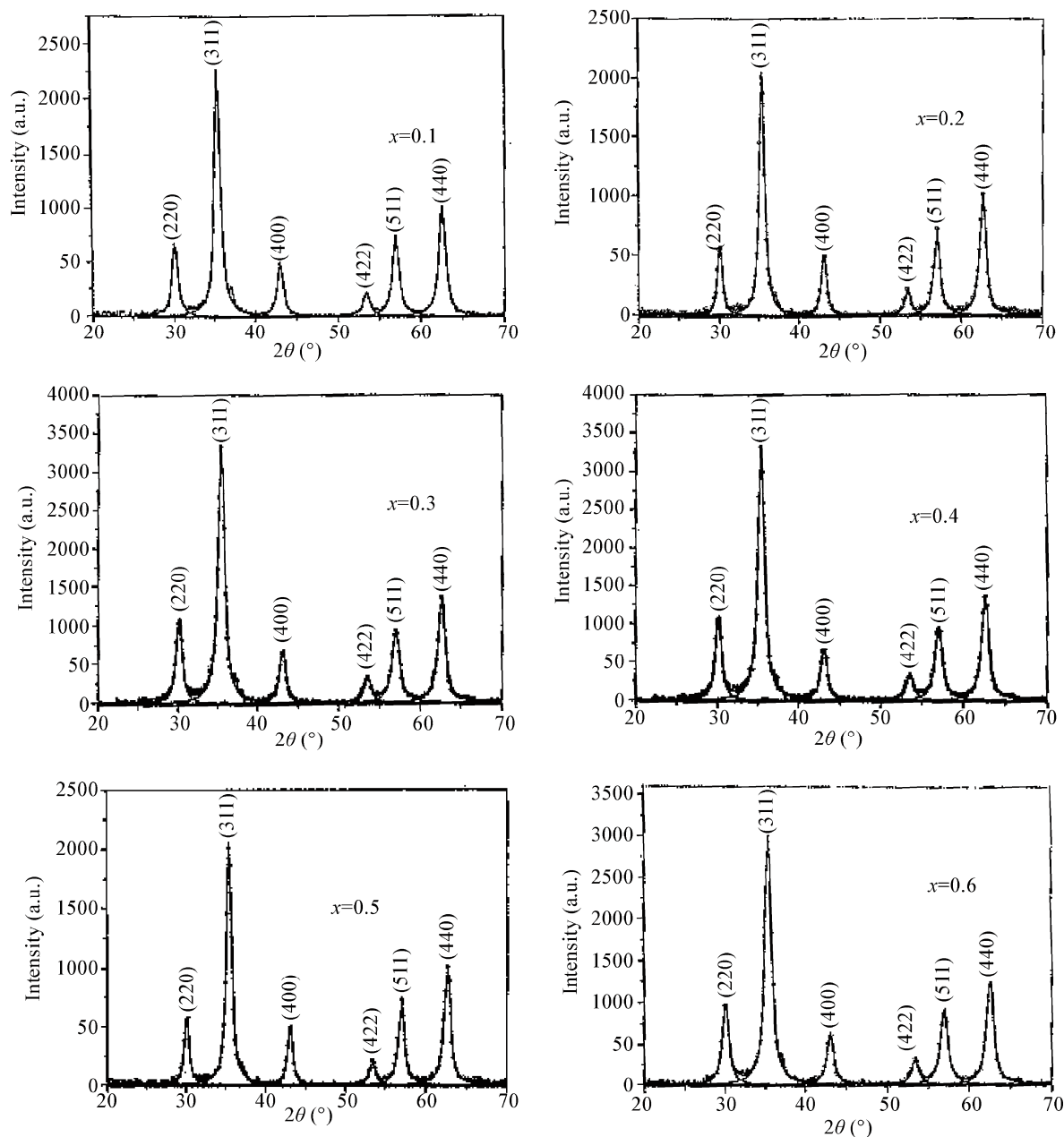


Fig. 1 X-ray diffraction patterns of  $\text{Zn}_{1-x}\text{Co}_x\text{Fe}_2\text{O}_4$  ferrite ( $x = 0.1, 0.2, 0.3, 0.4, 0.5$  and  $0.6$ )

in this study are of spinel type cubic structure. To measure the diffusion coefficient of oxygen vacancies, the samples were annealed in an enriched oxygen atmosphere with pressure (0.29 atm.) at the temperature 550 °C for a cooling time of about 1 min.

### 3 Results and discussion

#### 3.1 Effect of temperature on the diffusion of oxygen vacancies for the $\text{Co}_{1-x}\text{Zn}_x\text{Fe}_2\text{O}_4$ ferrite

The diffusion coefficient of oxygen vacancies in  $\text{Co}_{1-x}\text{Zn}_x\text{Fe}_2\text{O}_4$  ferrite (where  $x = 0.1, 0.2, 0.3, 0.4, 0.5$  and  $0.6$ ) as a function of temperature is illustrated in Fig. 2. The coefficient can be estimated from the relation [9].

$$\sigma_{dc} = (Ne^2D / k_B T) \quad (1)$$

where  $\sigma_{dc}$  is the dc electrical conductivity,  $N$  the number of atoms/cm<sup>3</sup>  $\cong 2 \times 10^{23}$ , and  $e$  the electronic charge. The diffusion coefficient ( $D$ ) increased significantly with increasing temperatures. The oxygen vacancies have been reported to accelerate densification during sintering process [10]. The diffusion of oxygen ions can usually only occur, however, if defects or structural vacancies are present in the structure, because otherwise there is no possibility of an anion jumping into a neighbouring lattice site. In our composition  $\text{Zn}^{2+}$  ions are substituted for  $\text{Co}^{2+}$  ions at the octahedral site, leading to migration of  $\text{Fe}^{3+}$  ions to replace  $\text{Zn}^{2+}$  ions at tetrahedral sites. This process creates lattice vacancies, since the valency of  $\text{Zn}^{2+}$  ions is less than that of  $\text{Fe}^{3+}$

ions. The temperature increases the mobility of vacancies, helping more oxygen vacancies to be diffused. The diffusion of oxygen vacancies increases with increasing  $\text{Zn}^{2+}$  ion concentrations [11]. This can be explained as follows: the migration of  $\text{Fe}^{3+}$  ions to replace  $\text{Zn}^{2+}$  at tetrahedral sites due to the substitution of  $\text{Zn}^{2+}$  for  $\text{Co}^{2+}$  ions at octahedral sites might cause the formation of anion vacancies. However, at higher Zn concentrations, the lattice vacancies are occupied by anions, leading to an increase in the number of anions vacancies and, hence, increasing in the diffusion of oxygen vacancies during sintering [12]. The dependence of the diffusion coefficient on temperature can be calculated from equation:

$$D = D_0 \exp\left(\frac{-E}{k_B T}\right) \quad (2)$$

where  $D_0 = \frac{k_B T \sigma_0}{Ne^2}$  is the pre-exponential factor,  $E$  is

the activation energy for the diffusion process and  $k_B$  is Boltzmann's constant. The logarithmic plot of Eq. (2), as shown in Fig. 2, gives a straight line for each composition. The straight line is broken at a certain critical temperature ( $T_c$ ), which is the magnetic transition above which the ferromagnetic material transforms to a paramagnetic [13,14]. The Curie temperature was determined for each composition. The activation energies for the diffusion process in the paramagnetic region ( $E_p$ ) on the left of  $T_c$  in Fig. 2 and in the ferromagnetic region ( $E_f$ ) on the right of  $T_c$  were also determined. The compositional dependence ( $x$ ) on the Curie temperature ( $T_c$ ) and lattice parameter ( $a$ ) is illustrated in Fig. 3. It is clear that  $T_c$  and lattice

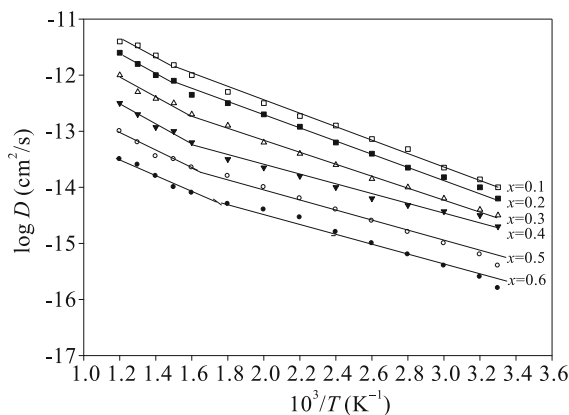


Fig. 2 Log ( $D$ ) as a function of temperature ( $T$ ) for  $\text{Zn}_{1-x}\text{Co}_x\text{Fe}_2\text{O}_4$  ferrite ( $x = 0.1, 0.2, 0.3, 0.4, 0.5$  and  $0.6$ )

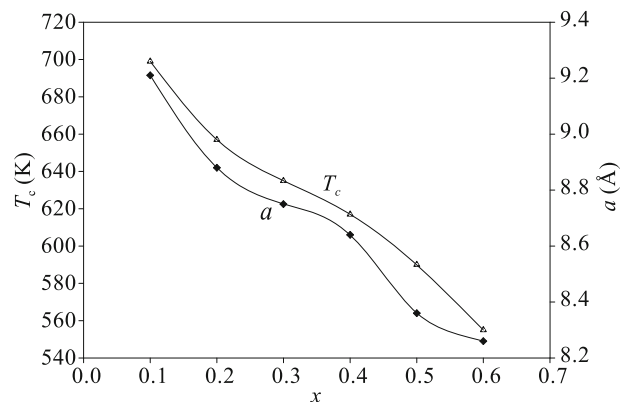


Fig. 3 Compositional dependence ( $x$ ) on Curie temperature ( $T_c$ ) and lattice parameter ( $a$ )

parameter decrease as the Zn ion content increases. The effect of  $x$  on the activation energies for the diffusion process ( $E_p$ ,  $E_f$ ) is shown in Fig. 4. The activation energy for the paramagnetic region is higher than that for the ferromagnetic region [15]. The activation energies increase as the  $Zn^{2+}$  increase.

### 3.2 Effect of Zinc concentration ( $x$ ) on the conductivity and jump length of electrons in $Co_{1-x}Zn_xFe_2O_4$ ferrite

The jump length  $L$  is determined from the relation below [10-11].

$$L = \frac{a\sqrt{2}}{4} \tag{3}$$

where  $a$  is the lattice parameter for each composition, calculated from the observed  $d$  values of the X-ray diffraction patterns as shown in Fig. 1. It is clear that the unit cell parameter  $a$  decreases with increasing  $x$ , approximately following Vegard's law. This can be expected in view of the fact that the ionic radius of  $0.83 \text{ \AA}$  for  $Zn^{2+}$  higher than that of  $0.74 \text{ \AA}$  for  $Co^{2+}$  and  $0.64 \text{ \AA}$  for  $Fe^{3+}$ . The variation of jump length  $L$  and dc conductivity at room temperature as a function of  $x$  in  $Co_{1-x}Zn_xFe_2O_4$  is shown in Fig. 5. This shows that the jump length and dc conductivity decrease with increasing Zn content. These results are explained by the assumption that  $Zn^{2+}$  enter the crystal structure in the tetrahedral sites. The interaction between  $Co^{2+}$  and  $Fe^{3+}$  at octahedral sites with increasing Zn concentration decrease the iron ion content. This interaction results in a corresponding decrease in the Cobalt and ferrous ions content at B sites, which is responsible for electrical conduction in the jump length [16,17]. The decrease of conductivity with increasing  $x$

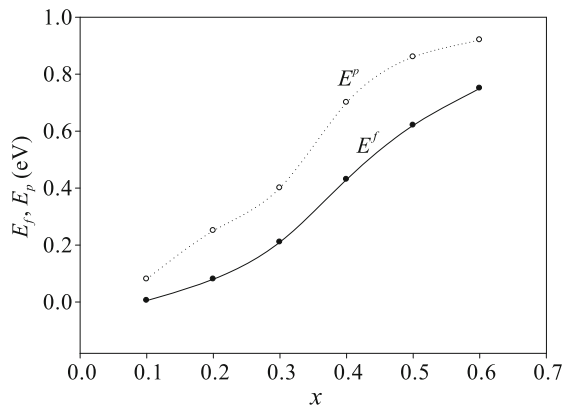


Fig. 4 Activation energies of the diffusion of oxygen vacancies in the given ferrite

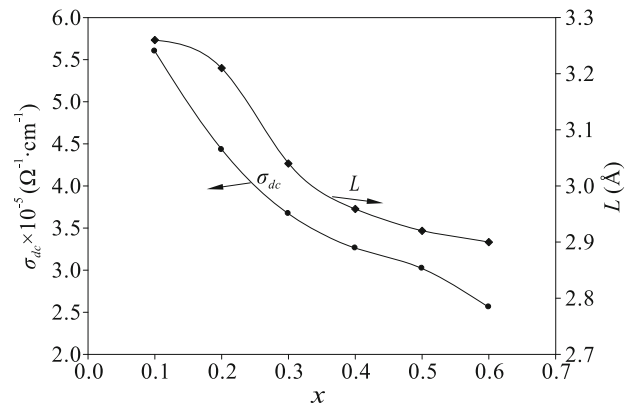


Fig. 5 Dependence of electrical conductivity ( $\sigma_{dc}$ ) and jump length ( $L$ ) o Zinc concentration.

is attributed to the following: nonmagnetic  $Zn^{2+}$  occupy positions in the B sublattice and this causes a decrease in both the A-B and B-B interaction forces [18], and the B-B interaction is responsible for conduction decrease.

### 3.3 Effect of $x$ on the jump rate ( $P$ ) of vacancies in $Zn_{1-x}Co_xFe_2O_4$ ferrite

The jump rate of vacancies in  $Zn_{1-x}Co_xFe_2O_4$  ( $x = 0.1, 0.2, 0.3, 0.4, 0.5$  and  $0.6$ ) was estimated from [13]

$$P = \frac{D}{a^2} \tag{4}$$

where  $a$  is the lattice parameter which was determined from X-ray diffraction patterns was in the previous work [19]. Figure 6 illustrates the dependence of  $P$  of vacancies and the apparent density ( $d$ ) on  $x$  at room temperature. It is clear that  $P$  and  $d$  increase as  $Zn^{2+}$  concentration increases. An increase in  $Zn^{2+}$  doping encourages the  $Fe^{3+}$  ions to occupy places at the A sites,

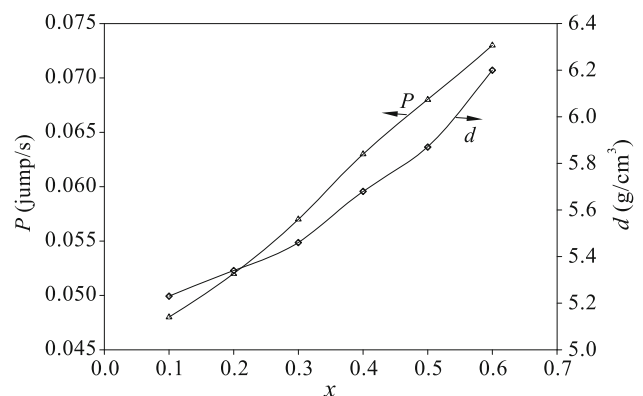


Fig. 6 Effect of Zinc concentration on the jump rate ( $P$ ) of vacancies and the apparent density ( $d$ ) at room temperature

leading to increases in the jump rate of vacancy through lattice vacancies which, in turn, influences the diffusion coefficient during the sintering process. Thus, a good relationship between the rate of jump vacancies and the diffusion coefficient during sintering (solid state reaction) exist. The lower valency of  $Zn^{2+}$  ions caused the formation of oxygen vacancies leading decrease in diffusion during sintering and increase in density. The  $Zn^{2+}$  addition increased the density, which is explained by the fact that  $Zn^{2+}$  higher atomic volume than  $Co^{2+}$  and  $Fe^{3+}$  ions.

### 3.4 Structural analysis

Figure 7 plots the variation of experimental and theoretical lattice parameters for  $Zn_{1-x}Co_xFe_2O_4$  ferrite. It is clear that the lattice parameters decrease with increasing Zn ions in place of  $Fe^{3+}$  ions at B sites. It is known that there is a correlation between the ionic radius and the lattice parameter. The theoretical lattice parameter ( $a_{th}$ ) was calculated by using the values of tetrahedral and octahedral radii  $r_A$ ,  $r_B$  and given by the following equation [16-20]:

$$a_{th} = \frac{8}{3\sqrt{3}} [((r_A + R_0) + \sqrt{3}(r_B + R_0))] \quad (5)$$

where  $R_0$  is the radius of the oxygen ion (1.32 Å). The cation distribution of the given samples should be known in order to calculate  $r_A$  and  $r_B$ . Accordingly, the cation distribution of the studied samples can be expressed in a general proposed form as follows:

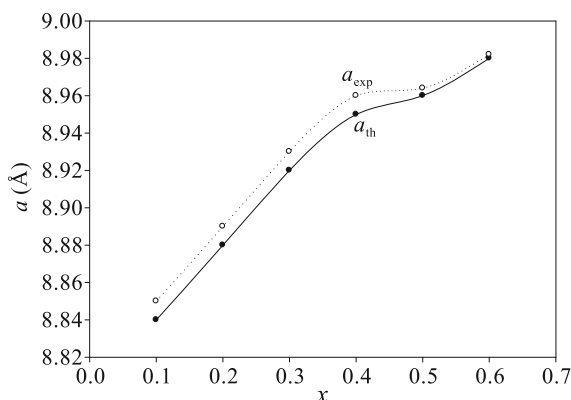
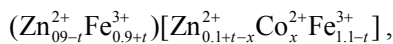


Fig. 7 Experimental and theoretical lattice parameter of the studied samples

where  $0.1 \leq x \leq 0.6$  and  $0.0 \leq t \leq 1.1$ . The ionic radius for each site is calculated from the following equation [16]:

$$r_A = (0.9 - t)r_{Zn^{2+}} + ((0.9 + t)r_{Fe^{3+}}),$$

$$r_B = [(0.1 + t - x)r_{Zn^{2+}} + xr_{Co^{2+}} + (1.1 - t)r_{Fe^{3+}}] / 2$$

It is noticed that the two values  $a_{th}$  and  $a_{exp}$  are nearly equal, which confirms our suggestion for the cation distribution. The values  $r_A$  and  $r_B$ , which depend on the assumption of cation distribution, are plotted against  $Zn^{2+}$  concentration as shown in Fig. 8. It can be seen that  $r_A$  increases and  $r_B$  decreases with increasing  $Zn^{2+}$  ion concentration. The replacement of  $Zn^{2+}$  ions by  $Co^{2+}$  ions leads to a decrease in  $r_B$ . Some of the  $Fe^{3+}$  ions migrate to A sites as a result of the substitution process and make some of  $Zn^{2+}$  ions transfer to B sites, which increases  $r_A$ .

### 4 Conclusion

(1) From the analysis of  $D$  and  $E$  of diffusion processes determined in our study, we conclude that in the studied samples the oxygen atoms diffuse through structural vacancies rather than thermal equilibrium vacancies in the oxygen sublattice.

(2) From X-ray analysis we can give a suggested cation distribution for the samples by adjusting the theoretical lattice parameter to be equal to the experimental one.

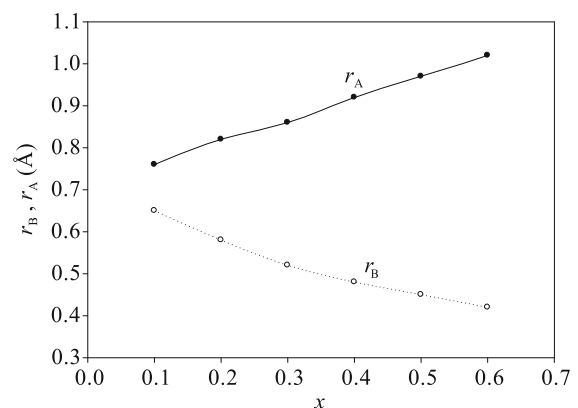


Fig. 8 Radius of octahedral sites ( $r_B$ ) and tetrahedral sites ( $r_A$ ) as a function of Zinc concentration

## References

- [1] Stoppls D. Developments in soft magnetic powder ferrites. *J Magn Magn Mater* 1996, **160**: 323-328.
- [2] Viswanathan B, Murthy VRK. Ferrite Materials: Science and Technology. New Delhi: Narosa Publishing House, 1990: 429-434.
- [3] Montiel H, Alvarez G, Gutiérrez MP, *et al.* Microwave absorption in Ni-Zn ferrites through the Curie transition. *J Alloys Compd* 2004, **369**:141-143.
- [4] Aoyama T, Hirota K, Yomaguch O. Characterization and low-temperature sintering of reactive Mn-Zn ferrite powder. *J Am Ceram Soc* 1996, **79**: 2792-2794.
- [5] Said MZ, Hemeda DM, Farag GZ, *et al.* Structural, electrical and infrared studies of Ni<sub>0.7</sub> Cd<sub>0.3</sub> Sm<sub>x</sub> Fe<sub>2-x</sub> O<sub>4</sub> ferrite. *Orient J Phys* 2009, **1**: 17-29.
- [6] Sileo EE, Rotelo R, Jacobo SE. Nickel-Zinc ferrites prepared by the citrate precursor method. *Phys B: Condens Matter* 2002, **320**: 257- 260.
- [7] Kumar A, Sharma S. Measurement of dielectric constant and loss factor of the dielectric material at microwave frequencies. *Progress Electromagn Res* 2007, **69**: 47-54.
- [8] Hemeda OM, El-Saadawy M, Barakat MM. The diffusion study of oxygen atoms in Co<sub>x/3</sub>Ni<sub>(5-x)/3</sub>Sb<sub>1/3</sub>Fe<sub>1</sub>O<sub>4</sub> ferrite. *J Magn Magn Mater* 2000, **219**: 73-77.
- [9] Wang WR, Wang SF, Lin YM. Low temperature sintering of (Zn<sub>1-x</sub> Mg<sub>x</sub>) TiO<sub>3</sub> microwave dielectric. *Ceram Int* 2005, **31**: 905-909.
- [10] Samaras D. The rotation of the magnetization in the BaCo<sub>2</sub>Fe<sub>16</sub>O<sub>27</sub> W- type hexagonal ferrite. *J Magn Magn Mater* 1989, **79**: 193-197.
- [11] El-Saadawy M. The diffusion coefficient of vacancies and jump length of electrons in nickel doped magnesium ferrite. *Orient J Phys* 2009, **1**: 9-16.
- [12] El-Saadawy M, Barakat MM. Effect of jump length of electrons on the physical properties of Mn-doped Co<sub>0.6</sub>Zn<sub>0.4</sub>Mn<sub>x</sub>Fe<sub>2-x</sub>O<sub>4</sub> ferrite. *J Magn Magn Mater* 2000, **213**: 309.
- [13] El-Saadawy M. The diffusion coefficient of vacancies and jump length of electrons in MgFe<sub>2-x</sub>Cr<sub>x</sub>O<sub>4</sub> ferrites. *J Int Ceram Rev* 2006, **55**: 18-21.
- [14] El-Saadawy M, Isam E. The diffusion coefficient of vacancies and jump length in Co<sub>x/3</sub> Ni<sub>(5-x)/3</sub>Sb<sub>1/3</sub>Fe<sub>1</sub>O<sub>4</sub> ferrites. *J Abhth Al- Yarmouk* 2002, **11**(2B): 205-212.
- [15] El-Saadawy M. Analysis of power loss at high frequency for ZnMn –W type hexagonal ferrites. *Orient J Phys* 2009, **1**(1-2): 31-38.
- [16] Hemeda OM, El-saadawy M. Effect of gamma irradiation on the structural properties and diffusion coefficient in Co-Zn ferrite. *J Magn Magn Mater* 2003, **256**: 63-68.
- [17] Lebourgeois R. Permeability mechanisms in high frequency polycrystalline ferrites. *J Magn Magn Mater*1996, **160**: 329-332.
- [18] Jin ZQ, Lin JP. Rapid thermal processing of magnetic materials. *J Phys D: Appl Phys* 2006, **39**: 227-244.
- [19] El-Saadawy M, Henaish MA. Thermal and electrical transport properties of Zn<sub>2-x</sub>Cu<sub>x</sub>Ba<sub>1</sub>Fe<sub>16</sub>O<sub>27</sub> hexagonal ferrite. *J Int Ceram Rev* 2001, **50**(3): 203-207.
- [20] Aoyama T, Hirota K, Yomaguch O. Magnetic properties of Mg<sub>x</sub>Zn<sub>1-x</sub>2W and Mn<sub>x</sub>Zn<sub>1-x</sub>2W ferrites. *J Am Ceram Soc* 1996, **79**(10): 2792-2794.